Role of Oxygen Vacancies on the Performance of Li[Ni0.5−xMn1.5+x]O4 (x = 0, 0.05, and 0.08) Spinel Cathodes for Lithium-Ion Batteries

ARTICLE *in* CHEMISTRY OF MATERIALS · JULY 2012

Impact Factor: 8.35 · DOI: 10.1021/cm301825h

6 AUTHORS, INCLUDING:

Jie Song
Massachusetts Institute of Technology
34 PUBLICATIONS **434** CITATIONS
SEE PROFILE

Yuhao Lu
29 PUBLICATIONS **846** CITATIONS
SEE PROFILE

CHEMISTRY OF MATERIALS

Article

pubs.acs.org/cm

Role of Oxygen Vacancies on the Performance of $Li[Ni_{0.5-x}Mn_{1.5+x}]O_4$ (x = 0, 0.05, and 0.08) Spinel Cathodes for Lithium-Ion Batteries

Jie Song, Dong Wook Shin, Yuhao Lu, Charles D. Amos, Arumugam Manthiram, and John B. Goodenough*

Materials Science and Engineering Program and Texas Materials Institute, The University of Texas at Austin, Austin, Texas 78712, United States

Supporting Information

ABSTRACT: Investigation of the high-voltage $Li[Ni_{0.5-x}Mn_{1.5+x}]O_4$ (x = 0, 0.05, 0.08) spinels prepared at temperatures of $T \leq 900$ °C and given different thermal treatments has shown that the solubility limit for oxygen vacancies in the disordered spinel phase is small at 600 °C. With x = 0, long-range ordering of Ni^{2+} and Mn^{4+} and elimination of all oxygen vacancies occurs after an anneal at 700 °C. Above 700 °C, a reversible transition from spinel to rock-salt is initiated, to accommodate oxygen loss. A sample quenched from 900 °C into liquid nitrogen traps some rock-salt second phase; the volume fraction of rock-salt phase decreases with oxygen uptake to 600 °C. However, upon slow cooling (1 °C min^{-1}) from 900 °C, the particles have time to eliminate most of the rock-salt phase by 700 °C; upon further cooling below 700 °C, the spinel phase and the oxygen gain are retained. However, the spinel phase retains oxygen vacancies and attendant Mn^{3+} with only short-range order of Ni and Mn. The rock-salt phase lowers sharply the electrochemical capacity of the quenched sample; but retention of Mn^{3+} in the slow-cooled sample improves the electrochemical performance relative to that of an oxygen-stoichiometric spinel formed by annealing at 700 °C. The Mn-rich $Li[Ni_{0.45}Mn_{1.55}]O_4$ sample annealed at 700 °C exhibits a segregation of a long-range-ordered spinel phase and a Ni-deficient spinel phase having a larger fraction near the particle surface. Removal of the Ni^{4+}/Ni^{2+} redox reactions from the surface stabilizes the electrochemical performance at 55 °C, but the problem of Mn^{2+} dissolution resulting from surface disproportionation of Mn^{3+} to Mn^{2+} and Mn^{4+} remains.

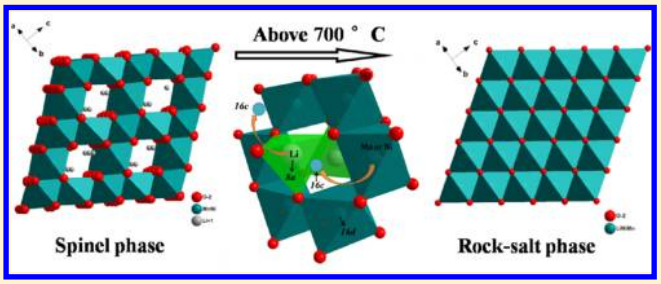

KEYWORDS: *Li-ion battery, spinel to rock-salt transition, high-voltage cathode, order−disorder*

INTRODUCTION

Much attention has been given to the spinel $Li[Ni_{0.5}Mn_{1.5}]O_4$ as a potential cathode for the Li-ion batteries, because it provides access to two nickel redox couples, Ni^{3+}/Ni^{2+} and Ni^{4+}/Ni^{3+}, at ~4.7 eV below the Fermi energy of a lithium anode with a negligible voltage step between the two couples. At 5.0 V versus Li^+/Li^0, oxygen is evolved and the electrolyte decomposes; however, more than 4.3 eV below Li, the spinel oxidizes the liquid-carbonate electrolyte unless a passivating solid-electrolyte interphase (SEI) layer is formed at the surface of the spinel.[1] These relative energies (see Figure 1) make it a challenge to stabilize high-voltage cycling of the spinel cathode, especially at elevated temperatures.

Various synthetic methods have been used to prepare nominal $Li[Ni_{0.5}Mn_{1.5}]O_4$ particles with different morphologies and sizes.[2−8] Ordering of the Ni^{2+} and the Mn^{4+} ions on the octahedral sites signals the presence of the stoichiometric spinel; loss of oxygen can introduce a rock-salt impurity phase, as well as the appearance of a shoulder at 4.0 V versus Li^+/Li^0 in the charge and discharge curves, which is indicative of the presence of Mn^{3+} in the spinel phase. The presence of an impurity rock-salt phase and a spinel phase containing Mn^{3+} is commonly observed after firing at 800−1000 °C.

Two approaches have been used to stabilize the charge/discharge cycling behavior: coating the spinel particles with Li-permeable oxides[9−13] and cation substitutions for Ni and/or Mn that produce a surface layer deficient in nickel.[14−22] The latter approach improves the electrochemical performances where trivalent dopants are used; but Ti^{4+} substitution for Mn^{4+} destroys the performance. However, the improved performance is normally accompanied by an increased width of the 4-V shoulder of the discharge and charge curves, even where the rock-salt phase is diminished.

The mechanism by which cation substitutions improve the electrochemical performance remains a subject of debate. Hagh et al.[23] and Xiao et al.[24] have proposed that the existence of Mn^{3+} is critical for an improved reversible Li extraction/insertion reaction at a higher cycle rate at 55 °C. On the other hand, surface Mn^{3+} ions are known to undergo a disproportionation reaction,

$$2Mn^{3+} = Mn^{2+} + Mn^{4+}$$

Received: June 12, 2012
Revised: July 9, 2012
Published: July 11, 2012

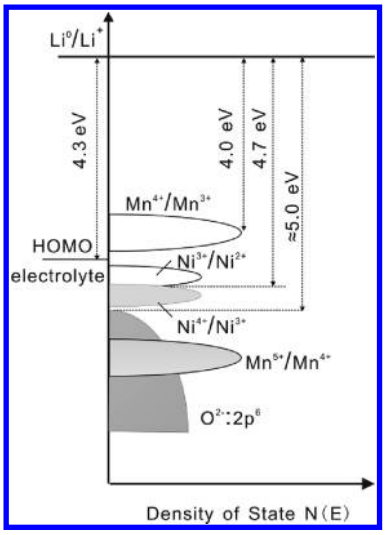

Figure 1. Schematic of the energy versus density of states plot, showing the relative positions of the redox couples in $Li[Ni_{0.5}Mn_{1.5}]O_4$ spinel and the highest occupied molecular orbital (HOMO) of carbonate electrolyte.

and the Mn^{2+} tends to dissolve in the electrolyte and migrate to the anode to degrade the cell. Zhong et al.[25] have shown that the greater the concentration of Mn^{3+} in the spinel, the greater the amount of soluble Mn^{2+} in the electrolyte. We[21,22] have argued that dopant M^{3+} ions segregate to the surface during synthesis to reduce the concentration of surface Ni^{2+} ions and that the surface Ni^{4+}/Ni^{3+} couple is responsible for oxidation of the electrolyte.

Since Mn^{3+} can be acting as a dopant M^{3+} ion, we have investigated the origin of the Mn^{3+} in $Li[Ni_{0.5}Mn_{1.5}]O_4$ and the temperatures at which Ni–Mn ordering and rock-salt-phase formation occur in $Li[Ni_{0.5-x}Mn_{1.5+x}]O_4$ (x = 0, 0.05, 0.08) by carefully controlling the cooling rate after calcinations in air and varying the Mn/Ni ratio to create different Mn^{3+} concentrations and degrees of structural ordering in the spinel. The role of oxygen vacancies in a reversible transition from spinel to rock-salt and in Ni–Mn ordering in the $Li[Ni_{0.5}Mn_{1.5}]O_4$ system has been clarified. Superior electrochemical performance of the Mn-rich samples has been achieved by elimination of the rock-salt phase and reduction of the Ni concentration at the surface.

EXPERIMENTAL SECTION

The spinels $Li[Ni_{0.5-x}Mn_{1.5+x}]O_4$ (x = 0, 0.05, 0.08) were prepared via the solid-state reaction of lithium hydroxide and nickel–manganese hydroxides, which were coprecipitated from aqueous solution of $Ni(NO_3)_2{\cdot}6H_2O$ and $Mn(NO_3)_2$ (50% solution) with NaOH solution and a specified amount of NH_4OH as a chelating agent. The precipitate was filtered and washed with distilled water and then dried at 110 °C. The obtained hydroxides were thoroughly mixed with the stoichiometric amount of $LiOH{\cdot}H_2O$ and pressed into pellets. Solid-state reaction was performed in air at 600 °C for 6 h. The pellets were ground, and new pellets were pressed and heated at 900 °C for 12 h. The samples were cooled from 900 °C at different rates: those cooled at a rate of 10 °C min^{-1} from 900 °C are called "fast-cooled samples" and those cooled at a rate of 1 °C min^{-1} are called "slow-cooled samples". Samples annealed at 700 °C for 48 h in air are called "annealed samples". Quenched samples were prepared by plunging the pellets into liquid nitrogen from 600 or 900 °C.

The thermogravimetic (TG) analyses were collected on a Perkin–Elmer TGA 7 system in flowing air. X-ray diffraction (XRD) patterns were step-scan-recorded on a Philips X-ray diffractometer equipped with Cu Kα radiation. Raman spectra were obtained with a Renishaw inVia Raman microscope with a 442-nm blue laser beam. X-ray photoelectron spectroscopy (XPS) data were acquired with a Kratos AXIS 165 Multitechnique Electron Spectrometer with a monochromatic Al Kα (1486.6 eV) source (Manchester, U.K.). The depth profiles of the cation concentration from the surface were examined by time-of-flight secondary-ion mass spectroscopy (TOF-SIMS) (Perkin–Elmer, Model ULVAC-PHI TFS2000 system equipped with a Bi-ion source) by sputtering pulsed 15 keV O^+ beams.

Electrochemical performances were evaluated with CR2032 coin half-cells composed of the nominal spinel cathode and metallic-lithium anode with 1 mol L^{-1} $LiPF_6$ in 1:1 diethyl carbonate/ethylene carbonate electrolyte and Celgard polypropylene separators. The cathodes were prepared by mixing 75 wt % active material with 20 wt % acetylene black and 5 wt % polytetrafluoroethylene (PTFE) binder; the mixture was rolled into thin sheets and punched into circular electrodes 0.8 cm in diameter. The typical electrode mass was 4–8 mg. All coin cells were assembled in an argon-filled glovebox. The cells were galvanostatically cycled under different current densities and different temperatures (room temperature and 55 °C) between 3.50 V and 4.95 V.

RESULTS

Figure 2 shows heating and cooling TG data taken at a rate of 10 °C min^{-1} for nominal $Li[Ni_{0.5}Mn_{1.5}]O_4$ after the four

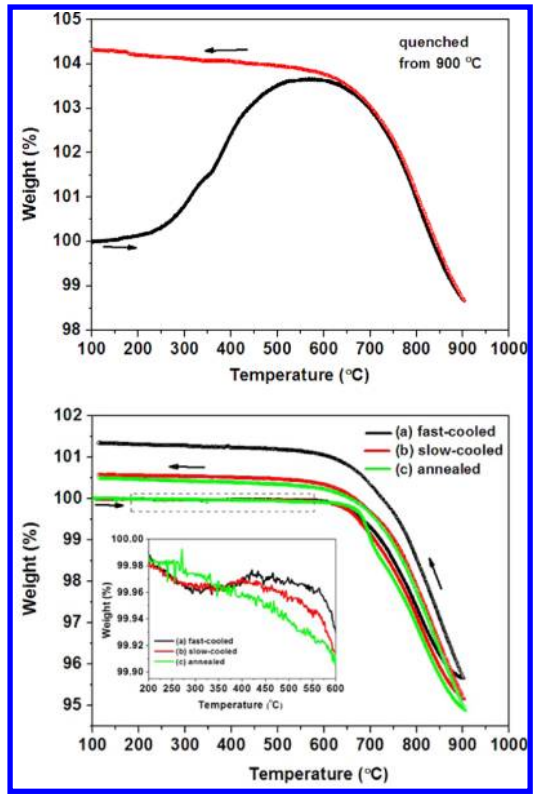

Figure 2. Thermogravimetric (TG) curves of the quenched, fast-cooled (10 °C min^{-1}), and slow-cooled (1 °C min^{-1}) samples from 900 °C, and annealed (at 700 °C) $Li[Ni_{0.5}Mn_{1.5}]O_4$ under air flow; the heating and cooling rates were 10 °C min^{-1}. The insert shows the details of TG analysis curves in the interval of 200 °C < T < 600 °C.

thermal treatments. The samples quenched from 900 °C show, upon heating, an initial weight gain between 250 and 600 °C, followed by a slight change in weight up to 700 °C, above which a sharp weight loss is observed. The weight loss above 700 °C is reversible and the weight at 700 °C is retained to room temperature to give a final weight ~5% greater than the

dx.doi.org/10.1021/cm301825h | Chem. Mater. 2012, 24, 3101–3109

starting weight of the quenched sample. A reversible weight loss in air indicates that oxygen is being lost and regained. We will show that (i) the increase in weight loss upon heating above 700 °C is the result of the growth of a rock-salt second phase formed above 700 °C, (ii) a disordered spinel is synthesized at 600 °C, and (iii) an ordered, oxygen-stoichiometric phase is formed in the interval of 600 °C < $T \leq$ 700 °C. In order to verify and follow the presence of a rock-salt second phase and the solubility of oxygen vacancies in the spinel phase, we performed room-temperature powder X-ray diffraction (XRD) and Raman spectroscopy on all samples and correlated the structural data with electrochemical data. Similar experiments were performed on $Li[Ni_{0.45}Mn_{1.55}]O_4$.

The nominal spinel $Li[Ni_{0.5}Mn_{1.5}]O_4$ is cubic with Li on the tetrahedral sites of the structure. With disordered Ni and Mn on the octahedral sites, the cubic spinels have the space group $Fd\bar{3}m$, but the ordering of Ni^{2+} and Mn^{4+} in $Li[Ni_{0.5}Mn_{1.5}]O_4$ gives the space group $P4_332$.[26,27] Since the Mn-rich $Li[Ni_{0.5-x}Mn_{1.5+x}]O_4$ (x = 0.05, 0.08) samples show similar structural and electrochemical properties, all Mn-rich results correspond to the $Li[Ni_{0.45}Mn_{1.55}]O_4$ in this paper. Figure 3 compares the room-temperature XRD patterns of the $Li[Ni_{0.5}Mn_{1.5}]O_4$ and $Li[Ni_{0.45}Mn_{1.55}]O_4$ samples after different thermal treatments. All patterns exhibit a cubic spinel structure. Weak reflections observed at 2θ = 37.6°, 43.7°, and 63.5° in $Li[Ni_{0.5}Mn_{1.5}]O_4$ samples are from the impurity phase, which is a cation-rich rock-salt phase; these reflections are reduced significantly in the Mn-rich $Li[Ni_{0.45}Mn_{1.55}]O_4$ samples and are absent in all samples annealed at 700 °C. The diffraction patterns of both $Li[Ni_{0.5}Mn_{1.5}]O_4$ and $Li[Ni_{0.45}Mn_{1.55}]O_4$ samples annealed at 700 °C have been indexed in the cubic $P4_332$ symmetry, rather than to the $Fd\bar{3}m$ space group, to account for the additional lines located at 2θ = 15.4°, 39.8°, 45.8°, and 57.6°, which are superlattice peaks, indicating Ni/Mn long-range ordering in the octahedral sites. Figure S1 in the Supporting Information shows a typical morphology of the spinel samples with a particle size of <5 μm. Figure S2 in the Supporting Information compares the lattice parameters of all the $Li[Ni_{0.5-x}Mn_{1.5+x}]O_4$ (x = 0, 0.05) samples with different thermal treatments. The lattice parameter of the samples annealed at 700 °C is smaller than that of the fast-cooled samples with the same composition; the Mn-rich samples with a composition of $Li[Ni_{0.45}Mn_{1.55}]O_4$ have larger lattice parameters than the $Li[Ni_{0.5}Mn_{1.5}]O_4$ samples with the same thermal history. The larger the lattice parameter, the greater the concentration of Mn^{3+} in the spinel phase, which can be derived from the 4-V shoulder in charge/discharge curves (see Table 1). The lattice parameters of the $Li[Ni_{0.45}Mn_{1.55}]O_4$ and $Li[Ni_{0.5}Mn_{1.5}]O_4$ samples annealed at 700 °C are very close, which indicates that they have the same Ni/Mn = 1/3 ordered phase, but there should be another Mn-rich spinel phase in the annealed $Li[Ni_{0.45}Mn_{1.55}]O_4$ sample to keep the Ni/Mn ratio at 0.45/1.55.

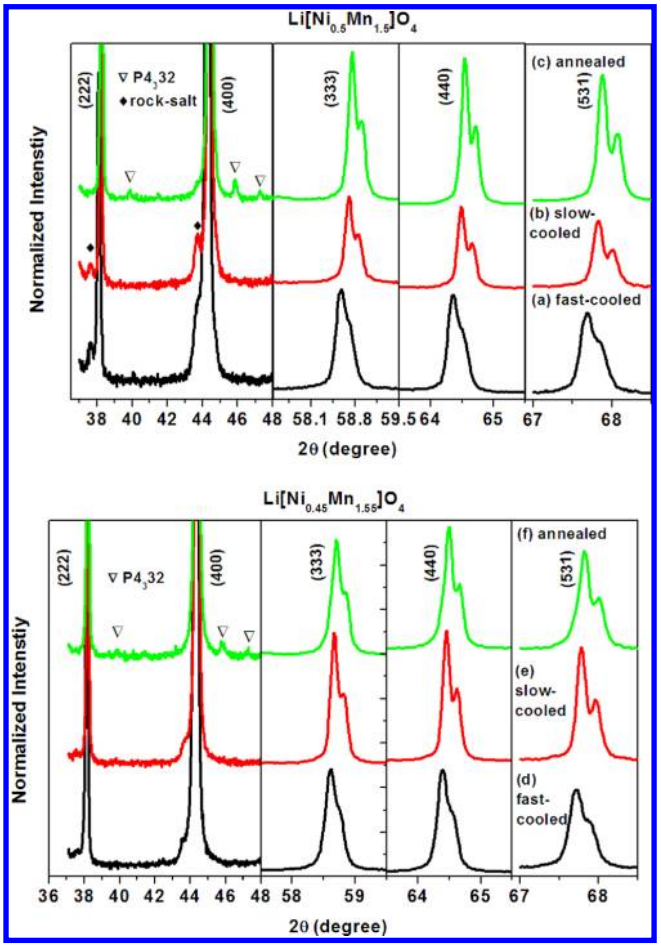

Figure 3. XRD patterns of (a) fast-cooled, (b) slow-cooled, and (c) annealed $Li[Ni_{0.5}Mn_{1.5}]O_4$, as well as XRD patterns of (d) fast-cooled, (e) slow-cooled, and (f) annealed $Li[Ni_{0.45}Mn_{1.55}]O_4$ samples.

Raman spectroscopy is a local probe analysis method that is sensitive to the crystal symmetry; it is a useful tool to determine the cation ordering, because the chemical contrast of Ni/Mn is poor in XRD. According to group theory, the number of expected Raman-active modes of the ordered spinel ($6A_1$+14E +$22F_2$) is larger than in the disordered spinel (A_g+E_g+$3F_{2\,g}$).[26] Figure 4 shows the Raman spectra of the $Li[Ni_{0.5}Mn_{1.5}]O_4$ and $Li[Ni_{0.45}Mn_{1.55}]O_4$ samples. The peaks at 630 cm^{-1} (symmetric Mn−O stretching vibration of MnO_6 groups) is assigned to the A_g mode, the lines at 490 and 390 cm^{-1} can be assigned to the Ni^{2+}−O stretching mode in the structure. The Raman spectrum of $Li[Ni_{0.5}Mn_{1.5}]O_4$ sample annealed at 700 °C exhibits extra peaks at 160, 218, and 239 cm^{-1} and a splitting of peaks in the 588−623 cm^{-1} region, which are characteristic of well-separated Ni and Mn sites resulting from the symmetry lowering in the ordered $P4_332$ structure.[26] The Raman spectra of the slow-cooled and annealed Mn-rich $Li[Ni_{0.45}Mn_{1.55}]O_4$ spinel both show features of Ni and Mn ordering at the octahedral sites, but there are no superlattice diffractions observed in the XRD of the slow-cooled $Li[Ni_{0.45}Mn_{1.55}]O_4$ (sample e in Figure 4). Apparently, there is short-range ordering in the slow-cooled $Li[Ni_{0.45}Mn_{1.55}]O_4$ spinel, with the fully ordered structure developing upon further annealing at 700 °C.

In order to clarify the onset temperature of the cation-rich rock-salt phase and of the elimination of Mn^{3+} ions with cation ordering, samples of $Li[Ni_{0.5}Mn_{1.5}]O_4$ were prepared in air at 600 °C; the XRD of this sample shows a well-defined $Fd\bar{3}m$ disordered spinel structure with no rock-salt impurity phase (Figure 5a). On the other hand, the XRD spectrum of the sample quenched into liquid nitrogen after sintering at 900 °C (Figure 5b) is well-refined with an $Fd\bar{3}m$ spinel and $Fm\bar{3}m$ rock-salt two-phase model. As argued by Wang et al.,[2] an abnormally strong intensity of the spinel (220) XRD peak may indicate antisite disorder associated with short-range Ni/Mn ordering. The lattice parameter of the spinel phase with

dx.doi.org/10.1021/cm301825h | Chem. Mater. 2012, 24, 3101−3109

Table 1. Comparison of Discharge Capacities and Mn^{3+} Contents in the $Li[Ni_{0.5}Mn_{1.5}]O_4$ and $Li[Ni_{0.45}Mn_{1.55}]O_4$ Samples

sample	Discharge Capacity (mAh g^{-1}) 4.7-V region[a]	4-V region[b]	amount of Mn^{3+} per formula unit of $Li[Ni_{0.5-x}Mn_{1.5+x}]O_4$[c]	ordering	lattice parameter (Å)
(a) fast-cooled $Li[Ni_{0.5}Mn_{1.5}]O_4$	107.2	22.8	0.16	disordered	8.1827
(b) slow-cooled $Li[Ni_{0.5}Mn_{1.5}]O_4$	115.7	12.7	0.09	disordered	8.1789
(c) annealed $Li[Ni_{0.5}Mn_{1.5}]O_4$	119.5	6.0	0.04	long-range ordered	8.1769
(d) fast-cooled $Li[Ni_{0.45}Mn_{1.55}]O_4$	109.3	23.0	0.16	disordered	8.1859
(e) slow-cooled $Li[Ni_{0.45}Mn_{1.55}]O_4$	114.2	20.5	0.14	short-range ordered	8.1831
(f) annealed $Li[Ni_{0.45}Mn_{1.55}]O_4$	120.3	18.4	0.13	long-range ordered	8.1771

[a]The 4.7-V region is the voltage range of 4.95−4.40 V. [b]The 4-V region is the voltage range of 4.40−3.50 V. [c]The amount of Mn^{3+} was calculated by the theoretical capacity of $Li[Ni_{0.5-x}Mn_{1.5+x}]O_4$ (x = 0, 0.05), which is ~147 mAh g^{-1}.

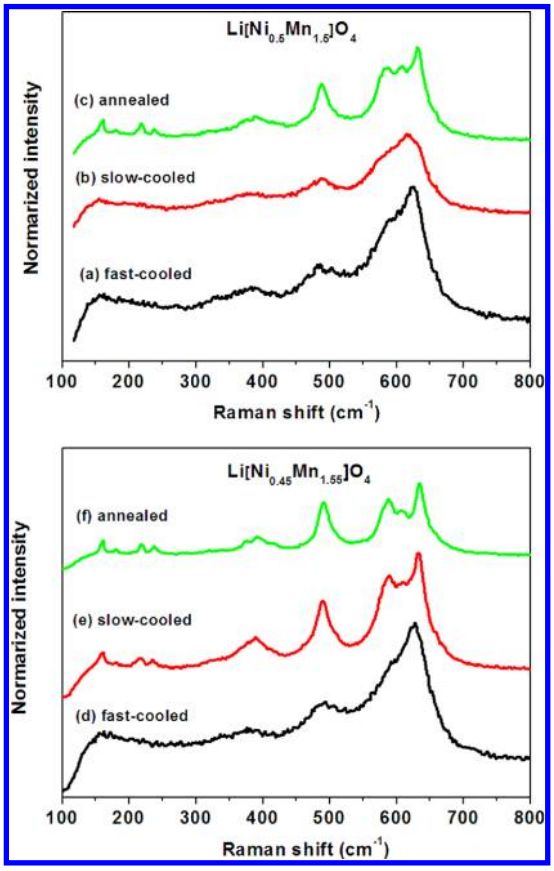

Figure 4. Raman spectra of (a) fast-cooled, (b) slow-cooled, and (c) annealed $Li[Ni_{0.5}Mn_{1.5}]O_4$, and Raman spectra of (d) fast-cooled, (e) slow-cooled, and (f) annealed $Li[Ni_{0.45}Mn_{1.55}]O_4$ samples.

apparent antisite disorder is larger than that of the ordered spinel phase. Figure 5c compares the XRD peaks in the 37−47° interval of the nominal $Li[Ni_{0.5}Mn_{1.5}]O_4$ samples after all the several thermal treatments. The data show that the fraction of the rock-salt phase decreases as the cooling process is slowed; it totally disappears after annealing at 700 °C. The transition from spinel to rock-salt phase is reversible, but the TG data are consistent with a first-order transition.

Since oxygen is lost from the surface of the sample, the rock-salt phase can be expected to grow from the surface with poor Li extraction/insertion from/into the rock-salt phase; we should expect the quenched sample to show little charge/discharge capacity. Figure 6a shows the expected small capacity, but also no evidence of a plateau characteristic of a spinel phase. Figure 6b shows the first two charge−discharge curves of the 600 °C-prepared $Li[Ni_{0.5}Mn_{1.5}]O_4$ with a large irreversible capacity loss in the first cycle. The 4-V shoulder (also see Figure 8, presented later in this work) indicates the existence of Mn^{3+} in the $Li[Ni_{0.5}Mn_{1.5}]O_4$ prepared at 600 °C. Charge−discharge profiles of the second cycle of the $Li[Ni_{0.5}Mn_{1.5}]O_4$ and $Li[Ni_{0.45}Mn_{1.55}]O_4$ samples collected at a low current rate (15 mA g^{-1}, C/10 rate) are presented in Figure 7. The fast-cooled and slow-cooled $Li[Ni_{0.5}Mn_{1.5}]O_4$ and $Li[Ni_{0.45}Mn_{1.55}]O_4$ show two distinct plateaus at ~4.7 V that are attributed to the Ni^{3+}/Ni^{2+} and Ni^{4+}/Ni^{3+} redox couples. In contrast, the 700 °C-annealed $Li[Ni_{0.5}Mn_{1.5}]O_4$ and $Li[Ni_{0.45}Mn_{1.55}]O_4$ cathodes with ordered structure show flat profiles at 4.75 V. Removal of the small voltage step between the Ni^{3+}/Ni^{2+} and Ni^{4+}/Ni^{3+} couples indicates that ordering of the Ni^{2+} creates a single Ni^{4+}/Ni^{2+} redox energy; the 4.75 V plateau is associated with the ordered Ni sites. The capacity of the 4-V shoulder, which is due to the Mn^{4+}/Mn^{3+} couple, increases as the cooling rate increases from 900 °C. The capacities in the 4-V and 4.7-V regions of all samples are summarized in Table 1. The cooling rate significantly affects the amount of Mn^{3+} ions in the $Li[Ni_{0.5}Mn_{1.5}]O_4$ samples. For instance, the fast-cooled $Li[Ni_{0.5}Mn_{1.5}]O_4$ (sample (a) of Table 1) delivers a discharge capacity of 22.8 mAh g^{-1} in the 4-V region, corresponding to 0.16 Mn^{3+} ions per formula unit; however, in the Mn-rich $Li[Ni_{0.45}Mn_{1.55}]O_4$ samples, the effect of the cooling rate is much smaller. Slow cooling and annealing of the Mn-rich samples only reduces the Mn^{3+} concentration by a small amount. The capacity at 4.75 V increases as the cooling rate decreases, which means greater access to active Ni^{4+}/Ni^{2+} redox couples on ordered Ni, in agreement with the elimination of the rock-salt phase and a larger volume fraction of ordered Ni^{2+}, as shown in the XRD analysis.

In the Mn-rich samples, the 4-V plateau splits into two quite reversible shoulders at ~4.0 V and ~4.25−4.3 V (Figure 8); moreover, the voltage difference of the two split shoulders increases with Mn/Ni ordering from the fast-cooled sample to the annealed sample. The XRD and Raman data have shown short-range and long-range ordered structures in slow-cooled and annealed Mn-rich $Li[Ni_{0.45}Mn_{1.55}]O_4$ samples. The shoulder at 4.3 V is clearly associated with the ordered phase. Since the ordered phase keeps the Mn/Ni ratio at 3:1, there should be another unidentified spinel phase with a Mn/Ni ratio greater than 3:1 that is responsible for the shoulder at 4.0 V. XPS Ni 2p spectra were recorded on the powders of all samples

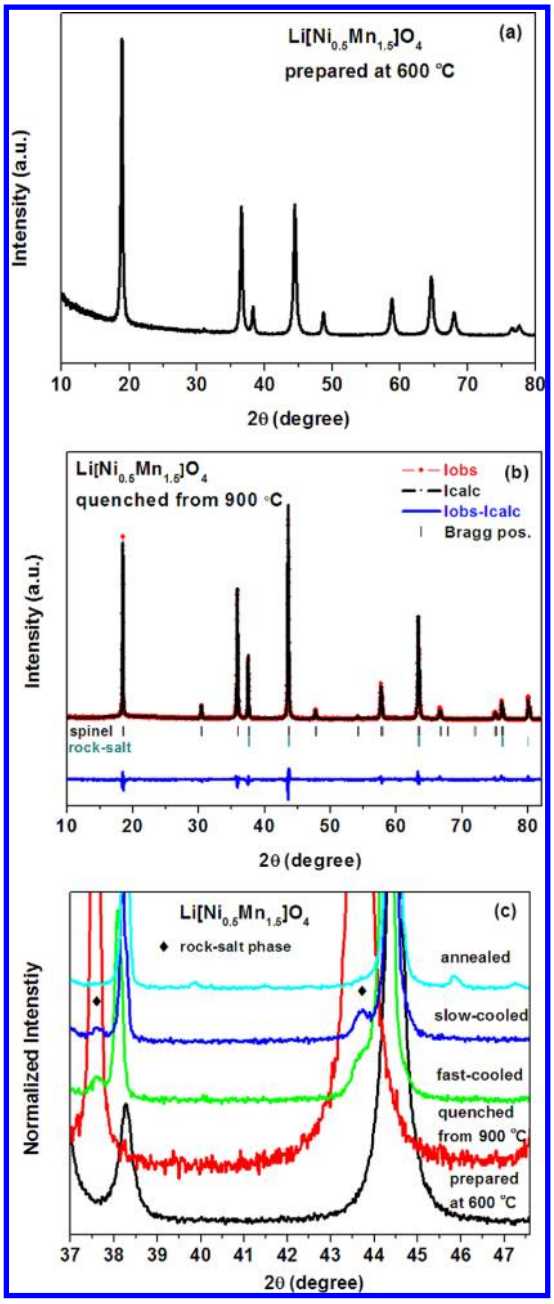

Figure 5. (a) XRD pattern of $Li[Ni_{0.5}Mn_{1.5}]O_4$ prepared at 600 °C, (b) refined XRD pattern of the $Li[Ni_{0.5}Mn_{1.5}]O_4$ quenched from 900 °C, and (c) XRD patterns of the $Li[Ni_{0.5}Mn_{1.5}]O_4$ samples prepared at 600 °C, quenched from 900 °C, fast-cooled, slow-cooled, and annealed in the 37°−48° interval, showing the evolution of the rock-salt phase.

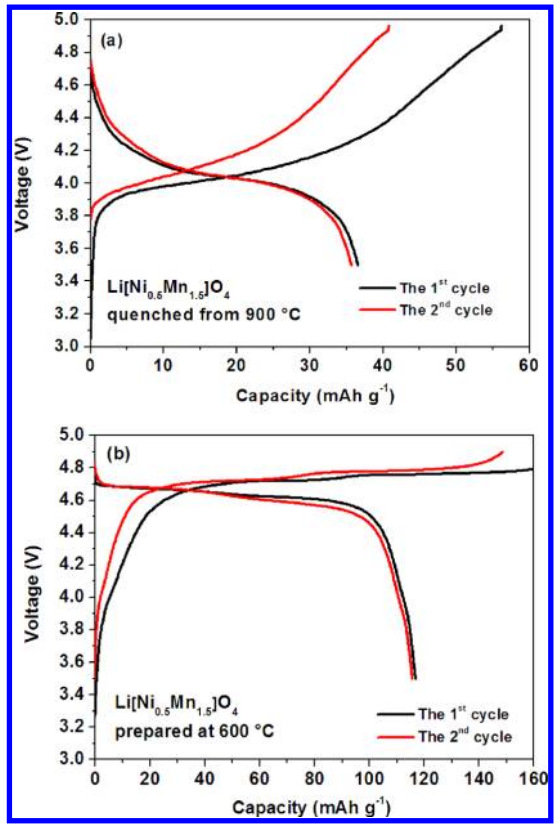

Figure 6. Charge and discharge profiles for the first two cycles of the $Li[Ni_{0.5}Mn_{1.5}]O_4$ samples (a) quenched from 900 °C and (b) prepared at 600 °C.

pressed on conductive carbon tape (see Figure S3 in the Supporting Information); a small shoulder at higher binding energy of the Ni $2p_{3/2}$ line occurs in samples showing a 4.3-V shoulder.

Figure 9 shows the cycling performance of the $Li[Ni_{0.5}Mn_{1.5}]O_4$ and $Li[Ni_{0.45}Mn_{1.55}]O_4$ samples at room temperature and 55 °C. At room temperature, the $Li[Ni_{0.5}Mn_{1.5}]O_4$ and Mn-rich $Li[Ni_{0.45}Mn_{1.55}]O_4$ retain, respectively, 92%−94% and 95%−97% capacity over 100 cycles, and their Coulombic efficiencies are as high as 99% after the initial several cycles. The capacities of the $Li[Ni_{0.5}Mn_{1.5}]O_4$ samples fade fast when cycled at 55 °C; the fast-cooled, slow-cooled, and annealed $Li[Ni_{0.5}Mn_{1.5}]O_4$ samples retained only 64%, 67%, and 63% capacity, respectively, over 100 cycles. The Mn-rich $Li[Ni_{0.45}Mn_{1.55}]O_4$ samples deliver an improved cycling performance at 55 °C; the retentions are ~93% over 100 cycles with a Coulombic efficiency of 95%. Figure S4 in the Supporting Information shows the charge and discharge curves of all samples at high-temperature cycling. The capacity fade takes place mostly in the 4.7-V region of samples (a), (b), and (c) where the Ni^{2+} ions are being oxidized to Ni^{4+}.

The $Li[Ni_{0.5}Mn_{1.5}]O_4$ samples show good capacity retentions at room temperature, but they fade sharply at elevated temperature. XRD patterns (not shown) of $Li[Ni_{0.5}Mn_{1.5}]O_4$ samples taken before and after 100 cycles at 55 °C show little, if any, change, indicating that the elevated-temperature cycling performance is related to a surface reaction of the material with the electrolyte, not to the bulk properties.

Figure 10 shows the rate capability at room temperature of $Li[Ni_{0.5}Mn_{1.5}]O_4$ and Mn-rich $Li[Ni_{0.45}Mn_{1.55}]O_4$ samples at different discharge current densities while the charge current was kept constant at 0.2 C rate (1 C corresponds to 150 mA g^{-1}). The slow-cooled samples show the best rate capability among the three samples with the same composition. However, the improved rate capability depends on the removal of all of the rock-salt phase and the lack of long-range ordering between Mn^{4+} and Ni^{2+}. Moreover, the slow-cooled $Li[Ni_{0.45}Mn_{1.55}]O_4$ exhibits the highest discharge voltage plateau and capacity at high discharge current densities; for instance, the discharge capacity retentions are 85% and 67% of the 0.2 C capacity at 5 and 10 C, respectively.

Figure 11 shows the TOF-SIMS depth profiles of the slow-cooled $Li[Ni_{0.5-x}\ Mn_{1.5+x}]O_4$ (x = 0, 0.05) samples. The Mn-rich $Li[Ni_{0.45}Mn_{1.55}]O_4$ sample exhibits a lower concentration

dx.doi.org/10.1021/cm301825h | Chem. Mater. 2012, 24, 3101−3109

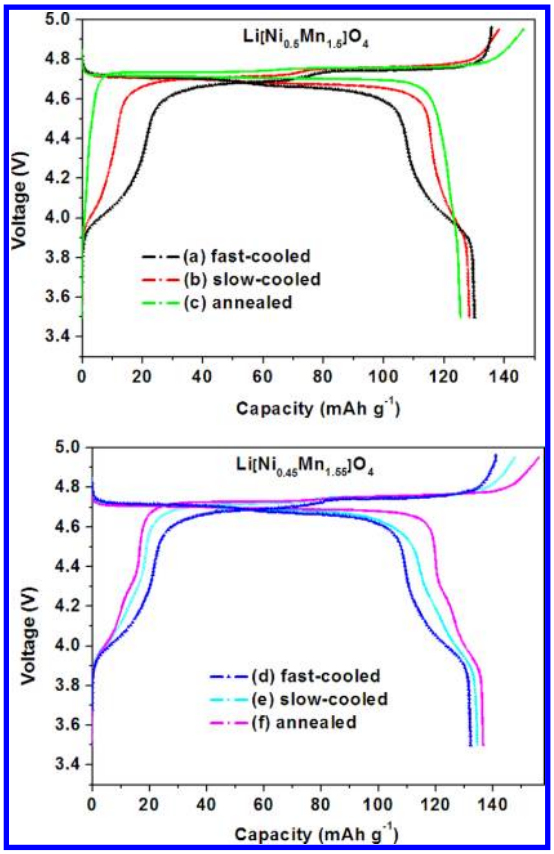

Figure 7. Charge and discharge curves of (a) fast-cooled, (b) slow-cooled, and (c) annealed $Li[Ni_{0.5}Mn_{1.5}]O_4$ and charge and discharge curves of (d) fast-cooled, (e) slow-cooled, and (f) annealed $Li[Ni_{0.45}Mn_{1.55}]O_4$ samples at the second cycle at low current density (15 mA g^{-1}, C/10 rate).

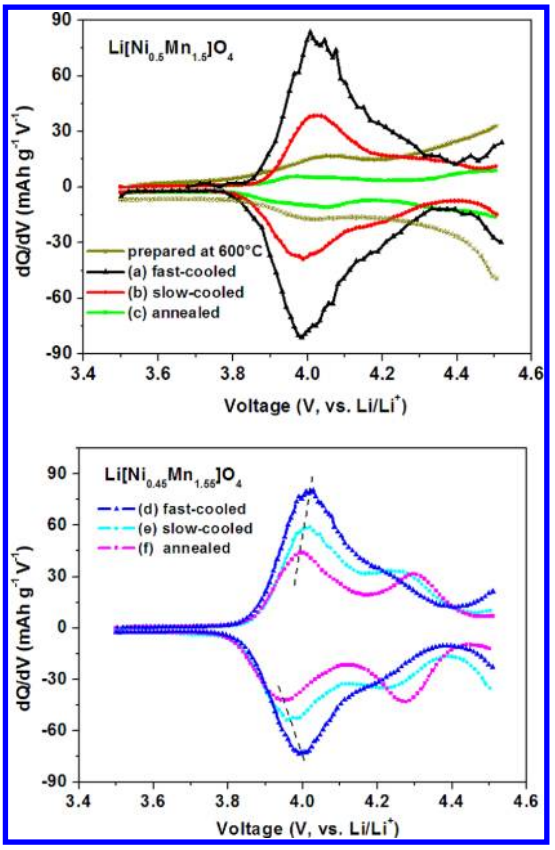

Figure 8. dQ/dV versus voltage in 4-V region of $Li[Ni_{0.5}Mn_{1.5}]O_4$ samples prepared at 600 °C ((a) fast-cooled, (b) slow-cooled, and (c) annealed) and dQ/dV versus voltage in 4-V region of $Li[Ni_{0.45}Mn_{1.55}]O_4$ ((d) fast-cooled, (e) slow-cooled, and (f) annealed samples at the second cycle).

of Ni near the surface, compared to that in the bulk. On the other hand, the $Li[Ni_{0.5}Mn_{1.5}]O_4$ sample exhibits a higher concentration of Ni near the surface.

3. DISCUSSION

A reversible loss of oxygen above 700 °C in air is accommodated by the formation of a rock-salt second phase that forms initially at the surface and grows into the bulk. Lithium is retained in the samples below 900 °C, so Mn^{3+} ions are formed to balance the charge change with O_2 evolution. The transition from spinel to rock-salt is reversible. Therefore, the oxygen uptake on slow cooling in air of $Li[Ni_{0.5}Mn_{1.5}]O_4$ from 900 °C to 700 °C allows time for elimination of most, if not all, of the rock-salt second phase, but not for conversion of short-range to long-range order of Ni^{2+} and Mn^{4+}, which is accompanied by elimination of all Mn^{3+} ions. Retention of some Mn^{3+} ions in a disordered spinel phase prepared at 600 °C shows that the disordered spinel phase can contain a small concentration of oxygen vacancies. Long annealing at 700 °C gives time not only for elimination of the rock-salt phase, but also for an ordering of the Ni^{2+} and Mn^{4+} ions, which eliminates all the absorbed oxygen vacancies. There is no obvious shoulder or redox reaction at 4.0 V in the charge/discharge curves in the $Li[Ni_{0.5}Mn_{1.5}]O_4$ spinel phase with ordered Ni^{2+} and Mn^{4+} obtained by an anneal in air at 700 °C.

As has been demonstrated with the $Li_{1+x}[Mn_2]O_4$ system,[27] the introduction of any Li^+ interstitial cations into the $Li[Mn_2]O_4$ spinel sites displaces all the tetrahedral-site Li^+ to the empty octahedral sites of the interstitial space of the spinel framework, thus creating a cation-deficient rock-salt phase with retention of the spinel framework. Upon extraction of Li at room temperature, the spinel phase is reformed with Li^+ returning to the interstitial tetrahedral sites of the framework. This transition is first-order and reversible at room temperature under an applied electric field. In $Li[Ni_{0.5}Mn_{1.5}]O_4$, the formation of the rock-salt phase requires a transfer of Ni and/or Mn to interstitial octahedral sites (*16c*), thus displacing the Li^+ from tetrahedral sites (*8a*) to octahedral sites (*16c*), the oxide ions retain a face-centered-cubic array (see Figure 12). Therefore, the rock-salt phase is only generated above 700 °C where the Ni and/or Mn become mobile; but at these temperatures, the spinel to rock-salt phase transition is reversible with changes in the concentration of oxygen vacancies.

How the weight changes upon the heating to 900 °C in air after samples have been given different thermal histories (Figure 2) is instructive. The sample quenched into liquid nitrogen after a 12-h anneal at 900 °C would contain not only a volume fraction of rock-salt phase, but a disordered spinel phase with a maximum 900 °C solid solution of oxygen vacancies. In this case, the weight gain upon heating in air begins above 250 °C (after the loss of absorbed water) with the uptake of oxygen in the spinel phase. Reduction of the volume fraction of the rock-salt phase may begin above ~325 °C until it is eliminated near 600 °C, but the transformation of the oxygen-deficient, disordered spinel phase to long-range order-

dx.doi.org/10.1021/cm301825h | *Chem. Mater.* 2012, 24, 3101−3109

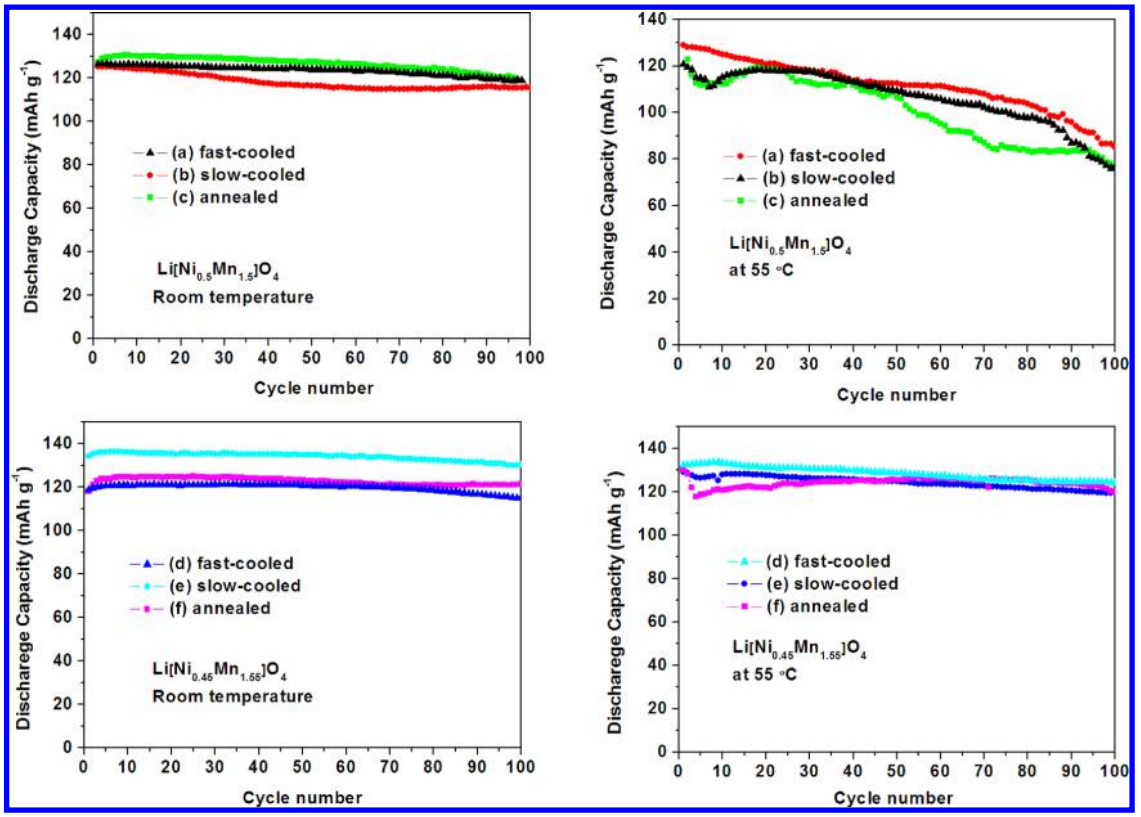

Figure 9. Cycling performances of (a) fast-cooled, (b) slow-cooled, and (c) annealed $Li[Ni_{0.5}Mn_{1.5}]O_4$ and cycling performances of (d) fast-cooled, (e) slow-cooled, and (f) annealed $Li[Ni_{0.45}Mn_{1.55}]O_4$ samples at room temperature and 55 °C. The charge and discharge current densities were 60 mA g^{-1}, and the voltage range was 3.50−4.95 V.

ing of Ni^{2+} and Mn^{4+} with elimination of the remaining oxygen vacancies in the spinel phase does not occur until ∼650 °C; moreover, 700 °C appears to be close to the upper temperature limit for the retention of the ordered spinel phase without a rock-salt second phase. At higher temperatures, the loss of oxygen is accommodated by reversible formation of the rock-salt phase. Upon thermal cycling to 900 °C, the sample spends little time at 900 °C, so the 900 °C equilibrium volume fraction of the rock-salt phase does not have time to be established throughout the sample. Therefore, upon cooling at 10 °C min^{-1}, the system is able to eliminate the existing rock-salt phase, which does not reform below 700 °C. Upon cooling to room temperature, the weight gain is retained; and at 300 °C, the equilibrium solid solution of oxygen vacancies in the spinel phase is achieved. As a result, the sample is ∼5% heavier at the end of the cycle than at the start.

On the other hand, samples annealed at 900 °C for 12 h have time to develop the equilibrium volume fraction of rock-salt phase throughout the sample. In this case, fast cooling (10 °C min^{-1}) does not allow time to eliminate all of the rock-salt phase or introduce long-range order in the spinel phase. Upon heating, elimination of the residual rock-salt phase begins, at ∼350 °C, becoming complete by 600 °C. The situation is similar in the slow-cooled samples, but the volume fraction of rock-salt phase is much smaller (not clearly visible to XRD) at the start of the run and is completely eliminated at 600 °C.

Although our fast-cooled $Li[Ni_{0.5}Mn_{1.5}]O_4$ samples exhibit a relatively poor electrochemical performance, despite a large Mn^{3+} concentration, this observation does not contradict the suggestion by the Amatucci group[28,29] that retention of Mn^{3+} in the spinel lattice provides a better rate capability of Li extraction/insertion, because of a higher electronic conductivity. In fact, the slow-cooled $Li[Ni_{0.45}Mn_{1.55}]O_4$ samples with a nearly absent volume fraction of the rock-salt phase gives the best electrochemical performance. The poor performance of the quenched and fast-cooled $Li[Ni_{0.5}Mn_{1.5}]O_4$ samples is a result of the large concentration of rock-salt phase that blocks Li^+ mobility.

Interestingly, the slow-cooled $Li[Ni_{0.45}Mn_{1.55}]O_4$ samples segregate into a Mn-rich, disordered spinel phase and a long-range-ordered spinel phase; moreover, they show two Mn^{4+}/Mn^{3+} redox couples: one at 4.0 V and the other at 4.3 V versus Li^+/Li^0. The disordered phase is known to have a Mn^{4+}/Mn^{3+} redox energy at 4.0 V. We have shown that the long-range-ordered spinel phase of $Li[Ni_{0.5}Mn_{1.5}]O_4$ obtained by annealing at 700 °C contains no Mn^{3+} and, therefore, no oxygen vacancies. Yet, the 4.3-V Mn^{4+}/Mn^{3+} couple is clearly associated with two spinel phases where one is long-range-ordered and the other is Mn-rich and disordered. A Mn^{4+}/Mn^{3+} energy at a higher voltage, 4.3 V versus 4.0 V, corresponds to a more-stable Mn^{4+}/Mn^{3+} couple than exists in a disordered phase containing oxygen vacancies; a more stable couple means more weakly bonded Mn^{4+}/Mn^{3+} sites (e.g., one bonding with more than one oxygen vacancy). Therefore, we are tempted to speculate that the elimination of oxygen vacancies from the long-range-ordered spinel phase introduces a larger concentration of oxygen vacancies at an interface phase between the ordered spinel and the Mn-rich disordered spinel.

From the TOF-SIMS data, the Mn-rich spinel contains fewer Ni atoms located near the surface. Since the Ni^{4+}/Ni^{3+} redox couple near 4.7 V versus Li^+/Li^0 is responsible for oxidation of the electrolyte to form a passivating SEI layer, our data suggest

dx.doi.org/10.1021/cm301825h | *Chem. Mater.* 2012, 24, 3101−3109

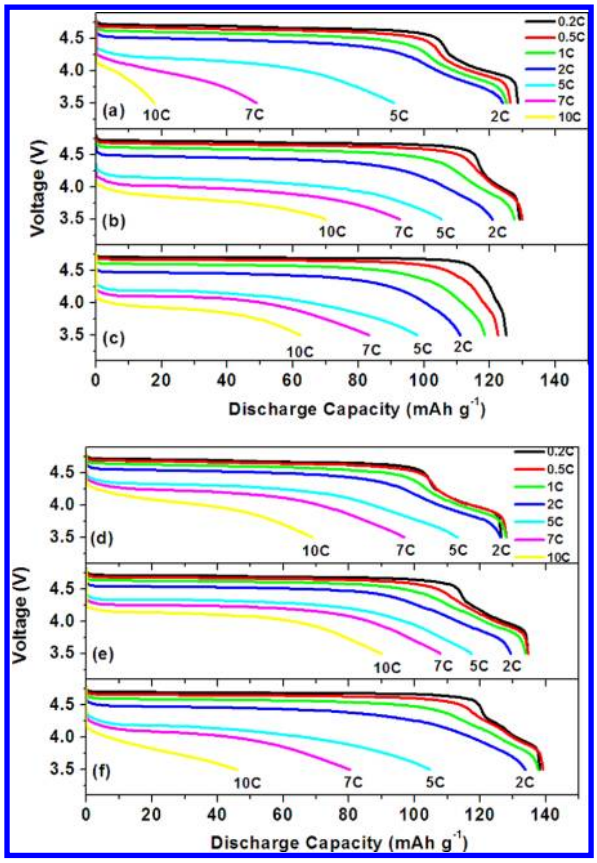

Figure 10. Discharge profiles of (a) fast-cooled, (b) slow-cooled, and (c) annealed $Li[Ni_{0.5}Mn_{1.5}]O_4$, and discharge profiles of (d) fast-cooled, (e) slow-cooled, and (f) annealed $Li[Ni_{0.45}Mn_{1.55}]O_4$ at various rates at room temperature. The charging current was kept at 0.2 C (1 C corresponds to 150 mA g^{-1}).

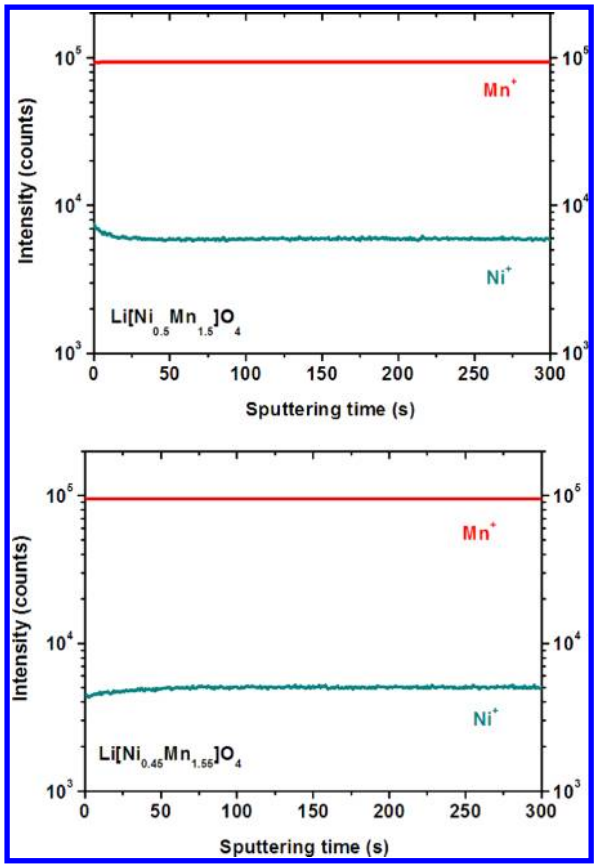

Figure 11. TOF-SIMS depth profiles of slow-cooled $Li[Ni_{0.5}Mn_{1.5}]O_4$ (top panel) and slow-cooled $Li[Ni_{0.45}Mn_{1.55}]O_4$ (bottom panel).

that reducing the surface Ni concentration at the surface stabilizes the spinel electrochemical performance at 55 °C. However, the problem of the disproportionation reaction, $2Mn^{3+} = Mn^{2+} + Mn^{4+}$, may still remain.

Previous reports have shown the appearance of a second phase in $Li[Ni_{0.5}Mn_{1.5}]O_4$ when the firing temperatures are above 750 °C.[4,28,30−33] Zhong et al.[30] first indexed the second phase as the rock-salt phase $Li_xNi_{1-x}O$ and proposed that it was unlikely that the rock-salt phase contains Mn, by comparison of lattice parameters of NiO and MnO. Cabana[34] found that the rock-salt phase contained Mn with a composition of $(Li_xMn_{0.66}Ni_{0.34})_yO$ by transmission electron microscopy (TEM) and energy-dispersive spectroscopy (EDS). Because of the close coherent scattering lengths of Ni and Mn, it is difficult to distinguish between the Ni and Mn atoms using XRD. Neutron diffractions and TEM measurements are needed to provide further information on the lithium distribution and compositions of the two phases.

4. CONCLUSIONS

The high-voltage spinel cathode $Li[Ni_{0.5}Mn_{1.5}]O_4$ retains Li upon firing in air at temperatures of $T \leq 900$ °C; any oxygen loss is charge-compensated by the reduction of Mn^{4+} to Mn^{3+}. Preparation at 600 °C gave a disordered spinel $Fd\bar{3}m$ phase containing a few oxygen vacancies and associated Mn^{3+} ions. An anneal at 700 °C orders the Ni^{2+} and Mn^{4+} ions on the octahedral sites long-range, with the elimination of Mn^{3+} ions and oxygen vacancies. Above 700 °C, a reversible oxygen loss sets in, which is accommodated by the formation of a rock-salt phase. The transition from spinel to rock-salt is reversible, via the reinsertion of oxygen upon slow cooling to 700 °C, and the oxygen regained is not lost upon further cooling to room temperature; however, too short of a time at 700 °C does not permit long-range ordering of the Ni and Mn with the elimination of oxygen vacancies. Oxygen vacancies and their associated Mn^{3+} are retained in a volume between short-range-ordered domains. Long-range ordering of Ni and Mn is formed in a narrow temperature interval (600 °C < $T \leq$ 700 °C).

A Mn-rich sample slow-cooled from 900 °C that has eliminated the rock-salt phase, but not the Mn^{3+} associated with a disordered spinel fraction separating domains of short-range order, gives the best electrochemical performance consistent with an enhancement by greater electronic conductivity while eliminating an obstructing rock-salt phase. Mn-rich samples, exemplified by $Li[Ni_{0.45}Mn_{1.55}]O_4$, retained Mn^{3+} in a single spinel phase prepared by annealing at 700 °C in air. However, the samples contained two spinel phases, one with long-range ordering of Ni^{2+} and Mn^{4+} and another Mn-rich spinel. The Mn-rich volume fraction exhibited two distinguishable Mn^{4+}/Mn^{3+} redox energies: one at 4.0 V and the other at 4.3 V, versus Li^+/Li^0. The 4.3-V redox energy is clearly identified with the existence of the long-range-ordered phase, which should not contain any Mn^{3+} ions. Therefore, we speculate that this couple is associated with an oxygen-poor interface phase between long-range-ordered domains or at the interface between the disordered, Mn-rich spinel and the long-range-ordered domains. The long-range ordered spinel phase gives a single voltage plateau at 4.75 V versus Li^+/Li^0; the state of charge of a

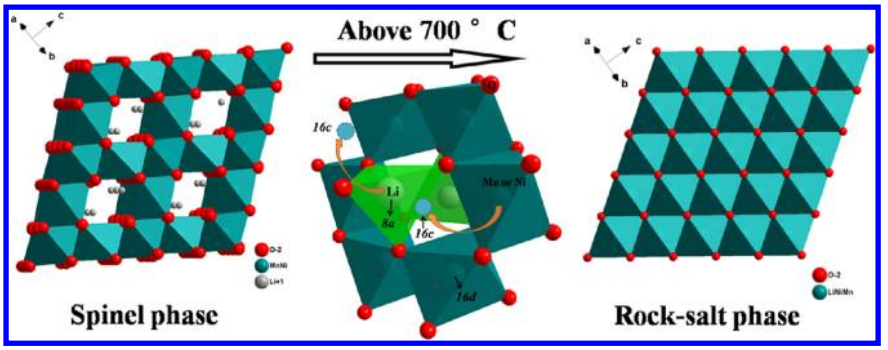

Figure 12. Schematic illustration of the transition from spinel to rock-salt phase above 700 °C. The migration of Ni and/or Mn to interstitial *16c* octahedral sites displaces the Li^+ from tetrahedral sites to octahedral sites. The transition from spinel to rock-salt phase is reversible with changes in the concentration of oxygen vacancies.

small voltage step from 4.7 V to 4.75 V signals the degree of short-range ordering in the sample.

The Mn-rich samples have a reduced Ni concentration at the surface and exhibit a better charge/discharge cycling at 55 °C, which signals that the Ni^{4+}/Ni^{2+} couple oxidizes the electrolyte. On the other hand, a larger Mn^{3+} concentration at the surface means a higher rate of disproportionation into Mn^{2+} and Mn^{4+} with Mn^{2+} dissolution; however, reduction of the surface Ni stabilizes the spinel against oxidation of the electrolyte at elevated temperatures (such as 55 °C).

■ ASSOCIATED CONTENT

Supporting Information

Typical SEM and lattice parameters of $Li[Ni_{0.5-x}Mn_{1.5+x}]O_4$ (x = 0, 0.05); XPS spectra; charge and discharge curves at 55 °C; and XRD, electrochemical data of $Li[Ni_{0.5}Mn_{1.5}]O_4$ quenched from 600 °C. This material is available free of charge via the Internet at http://pubs.acs.org.

■ AUTHOR INFORMATION

Corresponding Author

*Tel.: (512) 471-1646. Fax: (512) 471-7681. E-mail: jgoodenough@mail.utexas.edu.

Notes

The authors declare no competing financial interest.

■ ACKNOWLEDGMENTS

This work was supported by the Department of Energy Office of Basic Energy Science (Grant No. DE-SC0005397). The authors would like to thank Dr. Hengxing Ji for collecting Raman data and Dr. Hugo Celio for XPS data.

■ REFERENCES

(1) Goodenough, J. B.; Kim, Y. *Chem. Mater.* **2010**, *22*, 587.
(2) Wang, L. P.; Li, H.; Huang, X. J.; Baudrin, E. *Solid State Ionics* **2011**, *193*, 32.
(3) Kim, J. H.; Myung, S. T.; Yoon, C. S.; Kang, S. G.; Sun, Y. K. *Chem. Mater.* **2004**, *16*, 906.
(4) Shaju, K. M.; Bruce, P. G. *Dalton Trans.* **2008**, 5471.
(5) Liu, D.; Han, J.; Goodenough, J. B. *J. Power Sources* **2010**, *195*, 2918.
(6) Jo, M.; Lee, Y.-K.; Kim, K. M.; Cho, J. *J. Electrochem. Soc.* **2010**, *157*, A841.
(7) Cabana, J.; Zheng, H.; Shukla, A. K.; Kim, C.; Battaglia, V. S.; Kunduraci, M. *J. Electrochem. Soc.* **2011**, *158*, A997.
(8) Zhou, L.; Zhao, D.; Lou, X. *Angew. Chem., Int. Ed.* **2012**, *51*, 239.
(9) Sun, Y. K.; Lee, Y. S.; Yoshio, M.; Amine, K. *Electrochem. Solid State Lett.* **2002**, *5*, A99.
(10) Noguchi, T.; Yamazaki, I.; Numata, T.; Shirakata, M. *J. Power Sources* **2007**, *174*, 359.
(11) Kang, H. B.; Myung, S. T.; Amine, K.; Lee, S. M.; Sun, Y. K. *J. Power Sources* **2010**, *195*, 2023.
(12) Shi, J. Y.; Yi, C. W.; Kim, K. *J. Power Sources* **2010**, *195*, 6860.
(13) Liu, J.; Manthiram, A. *J. Electrochem. Soc.* **2009**, *156*, A833.
(14) Alcantara, R.; Jaraba, M.; Lavela, P.; Tirado, J. L.; Biensan, P.; de Guibert, A.; Jordy, C.; Peres, J. P. *Chem. Mater.* **2003**, *15*, 2376.
(15) Fey, G. T. K.; Lu, C. Z.; Kumar, T. P. *J. Power Sources* **2003**, *115*, 332.
(16) Alcantara, R.; Jaraba, M.; Lavela, P.; Lloris, J. M.; Vicente, C. P.; Tirado, J. L. *J. Electrochem. Soc.* **2005**, *152*, A13.
(17) Arunkumar, T. A.; Manthiram, A. *Electrochim. Acta* **2005**, *50*, 5568.
(18) Liu, J.; Manthiram, A. *J. Phys. Chem. C* **2009**, *113*, 15073.
(19) Zhong, G. B.; Wang, Y. Y.; Zhang, Z. C.; Chen, C. H. *Electrochim. Acta* **2011**, *56*, 6554.
(20) Oh, S. W.; Myung, S. T.; Kang, H. B.; Sun, Y. K. *J. Power Sources* **2009**, *189*, 752.
(21) Liu, D. Q.; Lu, Y. H.; Goodenough, J. B. *J. Electrochem. Soc.* **2010**, *157*, A1269.
(22) Shin, D. W.; Manthiram, A. *Electrochem. Commun.* **2011**, *13*, 1213.
(23) Hagh, N. M.; Cosandey, F.; Rangan, S.; Bartynski, R.; Amatucci, G. G. *J. Electrochem. Soc.* **2010**, *157*, A305.
(24) Xiao, J.; Chen, X.; Sushko, P. V.; Sushko, M. L.; Kovarik, L.; Feng, J.; Deng, Z.; Zheng, J.; Graff, G. L.; Nie, Z.; Choi, D.; Liu, J.; Zhang, J.-G.; Whittingham, M. S. *Adv. Mater.* **2012**, *24* (16), 2109–2116.
(25) Zhong, G. B.; Wang, Y. Y.; Yu, Y. Q.; Chen, C. H. *J. Power Sources* **2012**, *205*, 385.
(26) Amdouni, N.; Zaghib, K.; Gendron, F.; Mauger, A.; Julien, C. M. *Ionics* **2006**, *12*, 117.
(27) Thackeray, M. M. *Prog. Solid State Chem.* **1997**, *25*, 1.
(28) Kunduraci, M.; Amatucci, G. G. *J. Electrochem. Soc.* **2006**, *153*, A1345.
(29) Kunduraci, M.; Al-Sharab, J. F.; Amatucci, G. G. *Chem. Mater.* **2006**, *18*, 3585.
(30) Zhong, Q. M.; Bonakdarpour, A.; Zhang, M. J.; Gao, Y.; Dahn, J. R. *J. Electrochem. Soc.* **1997**, *144*, 205.
(31) Yi, T. F.; Xie, Y.; Ye, M. F.; Jiang, L. J.; Zhu, R. S.; Zhu, Y. R. *Ionics* **2011**, *17*, 383.
(32) Santhanam, R.; Rambabu, B. *J. Power Sources* **2010**, *195*, 5442.
(33) Pasero, D.; Reeves, N.; Pralong, V.; West, A. R. *J. Electrochem. Soc.* **2008**, *155*, A282.
(34) Cabana, J.; Casas-Cabanas, M.; Omenya, F.; Chernova, N. A.; Zeng, D.; Whittingham, M. S.; Grey, C. P. *Chem. Mater.* **2012**, DOI: 10.1021/cm301148d, Just accepted.